Eur. Phys. J. B (2020) 93: 60
https://doi.org/10.1140/epjb/e2020-100518-7

THE EUROPEAN PHYSICAL JOURNAL B

Regular Article

Efficient computation of Kubo conductivity for incommensurate 2D heterostructures*

Daniel Massatt[1], Stephen Carr[2], and Mitchell Luskin[3,a]

[1] Department of Statistics, University of Chicago, Chicago, IL 60615, USA
[2] Department of Physics, Harvard University, Cambridge, MA 02138, USA
[3] School of Mathematics, University of Minnesota, Minneapolis, MN 55455, USA

Received 24 October 2019 / Received in final form 29 January 2020
Published online 1 April 2020

Abstract. We introduce a numerical method for computing conductivity via the Kubo formula for incommensurate 2D bilayer heterostructures using a tight-binding framework. We begin by deriving the momentum space formulation and Kubo formula from the real space tight-binding model using the appropriate Bloch transformation operator. We further discuss the resulting algorithm along with its convergence rate and computational cost in terms of model parameters such as relaxation time and temperature. In particular, we show that for low frequencies, low temperature, and long relaxation times conductivity can be computed very efficiently using the momentum space algorithm for a wide class of materials. We then showcase our method by computing conductivity for twisted bilayer graphene (tBLG) for small twist angles.

1 Introduction

The electronic structure of incommensurate bilayers has attracted renewed interest after the discovery that stacking two layers of graphene on top of one another at a specific relative twist, called magic angle twisted bilayer graphene (tBLG), leads to electronic superconductivity [1]. *Twistronics*, the tuning of electronic structure by twisting stacks of 2D materials, gives a new set of parameters for tuning electronic structure, expanding the possible set of applications of these materials [2,3].

Incommensurate bilayers, especially for materials with small relative twist, typically require large system sizes to perform computations [2]. Further, given the weak van der Waals bonding between the materials, these systems are especially apt for studying via tight-binding models [4]. One approach for considering such materials is through the supercell approximation [5], though this can be prohibitively expensive at small angles, and leads to the computation of electronic properties for heterostructures with artificial strain since the system is not in a mechanical ground state. Real space electronic approaches have recently been developed that directly compute electronic observables such as the density of states or conductivity [6–8]. There is also extensive literature on momentum space or $k \cdot p$ approaches, which use the monolayers' Bloch bases [9,10].

In this paper, we begin with a real space tight-binding model and the real space Kubo formula [8] and transform these using the Bloch transform into a momentum space formulation and Kubo formula. Our approach extends the momentum space approach for the electronic density of states [11] to the computation of conductivity [11]. We note that a related formula for conductivity is discussed in works such as [12,13]. In these approaches, a Bloch basis is used but only at commensurate (supercell) twist angles and within the Dirac cone approximation. Even in monolayer graphene, the cone approximation provides accurate conductivity only at relatively low frequencies [14]. Other approaches for calculating optical conductivity in twisted bilayers have used density functional or tight-binding techniques in realspace [15,16], but are limited in their applicability at small twist angles. This is due to the increasing system size and required energy resolution to resolve spectral features as the twist angle decreases.

In this work, we focus on the rigorous transformation of the real space Kubo setting to the momentum space setting and on the convergence rate of the resulting algorithm. In doing so, one can treat arbitrary incommensurate angles by computing eigenvalues of small momentum matrices. We note that our approach is not restricted to only rigid tBLG: it can be extended to include mechanical relaxation effects [17–19], trilayer systems [20], or other 2D materials. We further demonstrate our results numerically by computing the conductivity of tBLG within the linear-response regime for several small twist angles and verifying fast convergence in terms of matrix truncation size.

The momentum space formulation leads to an algorithm with faster convergence than real space or supercell

* Contribution to the Topical Issue "Advances in Quasi-Periodic and Non-Commensurate Systems", edited by Tobias Stauber and Sigmund Kohler.

[a] e-mail: luskin@umn.edu

approaches with respect to a truncation radius r for certain materials. This causes the momentum formulation to have a significantly lower computational complexity compared to real space.

In Section 2, we define our real space formulation. In Section 3, we derive the momentum space formulation, in Section 4 we discuss the algorithm and convergence, and in Section 5 we present simulations on tBLG to demonstrate the algorithm.

2 Real space

We begin by defining the real space formulation for electronic structure in twisted 2D bilayers. Each layer, or sheet, is periodic in this model, so we define them with respect to Bravais lattices with bases generated by the columns of A_j for $j = 1, 2$ by

$$\mathcal{R}_j = A_j\mathbb{Z}^2, \quad j \in \{1, 2\}$$

with corresponding unit cells

$$\Gamma_j = A_j[0, 1)^2.$$

Each sheet has a finite orbital index set, $\mathcal{A}_j$, that labels the orbitals associated with each lattice point in the Bravais lattice. These orbitals can be centered anywhere within the unit cell to allow for the description of any 2D material, such as the honeycomb structures of graphene and MoS_2 or anisotropic structures such as black phosphorous.

For $\alpha, \alpha' \in \mathcal{A}_j$, we define the tight-binding interaction function, $h_{\alpha\alpha'} : \mathcal{R}_j \to \mathbb{R}$. For α, α' in opposite orbital index sets, we let $h_{\alpha\alpha'} : \mathbb{R}^2 \to \mathbb{R}$, which is defined over all $\mathbb{R}^2$ because of the incommensuration. We assume $h_{\alpha\alpha'}$ is smooth and exponentially localized in all its derivatives.

We then define the tight-binding degrees of freedom

$$\Omega = \cup_{j=1}^2 \mathcal{R}_j \times \mathcal{A}_j$$

and the finite domain

$$\Omega_r = \cup_{j=1}^2 (\mathcal{R}_j \cap B_r) \times \mathcal{A}_j,$$

where B_r is the ball of radius r centered at the origin. Our tight-binding Hamiltonian operator H is defined on the Hilbert space of vectors in $\ell^2(\Omega)$ and given by the expression

$$[H]_{R\alpha,R'\alpha'} = h_{\alpha\alpha'}(R - R') \tag{1}$$

for $R\alpha \in \mathcal{R}_j \times \mathcal{A}_j$ and $R'\alpha' \in \mathcal{R}_k \times \mathcal{A}_k$.

We next construct our Kubo formula for the real space model [8]. To begin, we let X_s be the position operator such that $(X_s)_{R\alpha} = R_s$ for $s \in \{1, 2\}$, and then recall the current operator

$$\begin{aligned}[X_s, H]_{R\alpha,R'\alpha'} &= (R - R')_s H_{R\alpha,R'\alpha'} \\ &= (R - R')_s h_{\alpha\alpha'}(R - R'). \end{aligned} \tag{2}$$

We define the current-current correlation measure $\mu_{ij}(E, E')$ [8] by the moments

$$\begin{aligned}\int \phi(E)\psi(E')\, d\mu_{ij}(E, E') \\ = \lim_{r\to\infty} \frac{1}{\#\Omega_r} \mathrm{Tr}_{\Omega_r}[\phi(H)[X_i, H]\psi(H)[X_j, H]]\end{aligned} \tag{3}$$

for all polynomials $\phi(E)$ and $\psi(E')$ (the current-current correlation measure is related to the current-current correlation density, $\rho_{ij}(E, E')$, by $d\mu_{ij}(E, E') = \rho_{ij}(E, E')\, dE\, dE'$). We construct an efficient algorithm by taking moments with respect to Chebyshev polynomials $T_k(E)$ [8]. Here Tr_{Ω_r} means trace over $\Omega_r \subset \Omega$ and $\#\Omega_r$ denotes the number of elements of the set Ω_r.

Given the Fermi-Dirac distribution

$$f_\beta(E) = \frac{1}{1 + e^{-\beta(E-E_F)}}$$

for E_F the Fermi energy, β the inverse temperature, and η the inverse dissipation time, we define the conductivity function

$$F(E, E') = \frac{ie^2}{\hbar(|\Gamma_1| + |\Gamma_2|)/2} \frac{f_\beta(E) - f_\beta(E')}{(E - E')(E - E' + \hbar\omega + i\eta)} \tag{4}$$

where ω is the frequency. The Kubo conductivity can then be given by [8]

$$\sigma_{ij} = \int F(E, E')\, d\mu_{ij}(E, E'). \tag{5}$$

We can formulate the conductivity in terms of the moments (3) by expanding the conductivity function (5) in Chebyshev polynomials

$$F(E, E') = \sum_{k_1,k_2=0}^{\infty} c_{k_1k_2}\, T_{k_1}(E)\, T_{k_2}(E') \tag{6}$$

where $T_k(E)$ denotes the kth Chebyshev polynomial defined through the three-term recurrence relation

$$T_0(x) = 1, \quad T_1(x) = x, \quad T_{k+1}(x) = 2x\, T_k(x) - T_{k-1}(x). \tag{7}$$

We developed a fast computational method for the conductivity (5) in [8] by a suitably truncated Chebyshev series, which significantly improves on the computational costs of a naive Chebyshev approximation. We also propose a rational approximation scheme for the low temperature regime $\eta^{-1/2} \lesssim \beta$ to remove the poles of the conductivity function (4). Chebyshev expansions will not be required in the momentum space formulation, as the Hamiltonian matrices will be far smaller than in the real space formulation, allowing for direct diagonalization.

3 Momentum space formulation

We next consider how to transform the real space Kubo formula to momentum space [11]. The reciprocal lattices basis vectors are generated by the columns of $2\pi A^{-T}$ giving the reciprocal lattice

$$\mathcal{R}_j^* = 2\pi A^{-T}\mathbb{Z}^2$$

with corresponding unit cells (Brillouin zones)

$$\Gamma_j^* = 2\pi A^{-T}[0,1)^2.$$

The Bloch waves for layer 1 defined by $e^{iq_1\cdot R_1}$ for $q_1 \in \Gamma_1^*$ and $R_1 \in \mathcal{R}_1$ can be equivalently represented by $e^{iK_2\cdot R_1}$ for $K_2 \in \mathcal{R}_2^*$ if the heterostructure is incommensurate, and similarly for layer 2. The momentum degrees of freedom space can thus be described in reciprocal space by [11]

$$\Omega^* = \Omega_1^* \cup \Omega_2^* := (\mathcal{R}_2^* \times \mathcal{A}_1) \cup (\mathcal{R}_1^* \times \mathcal{A}_2).$$

For wave functions $\psi \in \mathcal{R}_j \times \mathcal{A}_j$, we can define the Bloch transform

$$[\mathcal{G}_j\psi]_\alpha(q) = |\Gamma_j^*|^{-1/2} \sum_{R\in\mathcal{R}_j} e^{-iq\cdot R}\psi_R,$$

where $|\Gamma_j^*|$ denotes the area of Γ_j^*. Likewise, we define the Bloch transform over wave functions defined on the entire heterostructure Ω by the isomorphism $\mathcal{G} = (\mathcal{G}_1, \mathcal{G}_2)$, where $\mathcal{G}_1$ and $\mathcal{G}_2$ act on sheet 1 and sheet 2, respectively.

We now show that the momentum space operator with shift q is given by [11]

$$\begin{aligned}&[\widehat{H}(q)]_{K\alpha,K'\alpha'} = \delta_{KK'}|\Gamma_j^*|^{1/2}\mathcal{G}_j h_{\alpha\alpha'}(q+K),\\ &K\alpha \in \Omega_j^*,\ K'\alpha' \in \Omega_j^*\ j = 1,2\end{aligned} \tag{8}$$

for intralayer coupling and

$$\begin{aligned}&[\widehat{H}(q)]_{K\alpha,K'\alpha'} = \sqrt{|\Gamma_1^*|\cdot|\Gamma_2^*|}\hat{h}_{\alpha\alpha'}(q+K+K'),\\ &K\alpha \in \Omega_1^*,\ K'\alpha' \in \Omega_2^*\end{aligned} \tag{9}$$

for interlayer coupling where

$$\hat{h}_{\alpha\alpha'}(\xi) = \frac{1}{(2\pi)^2}\int h_{\alpha\alpha'}(x)e^{-ix\cdot\xi}dx.$$

The link between this momentum space operator and the real space operator is shown by applying the Bloch transform:

$$\mathcal{G}[H\psi]_\alpha(q) = \left[\widehat{H}(q)\xi(q)\right]_{0\alpha}, \tag{10}$$

where $\xi(q)$ is the wave function defined by $[\xi(q)]_{K\alpha} = \mathcal{G}\psi_\alpha(q+K)$. See Section A.1 for the derivation of (10). We define differentiation in momentum space ∂_j as the derivative with respect to q_j, where $q = (q_1, q_2)$. In particular, we consider the operator $\partial_j\widehat{H}(q)$. This in fact is the current operator in momentum space since

$$\begin{aligned}[\mathcal{G}_1[X_j,H]\psi]_\alpha(q) &= \left[\widehat{[X_j,H]}(q)\xi(q)\right]_{0\alpha}\\ &= i\left[\partial_j\widehat{H}(q)\xi(q)\right]_{0\alpha},\end{aligned} \tag{11}$$

where $[\xi(q)]_{K\alpha} = \mathcal{G}\psi_\alpha(q+K)$. See Section A.2 for the derivation. If A and B are operators over the Hilbert space with the two-center form of H and $[X_j, H]$

$$[A]_{R\alpha,R'\alpha'} = a_{\alpha\alpha'}(R-R') \text{ and } [B]_{R\alpha,R'\alpha'} = b_{\alpha\alpha'}(R-R'), \tag{12}$$

then $\widehat{AB}(q) = \widehat{A}(q)\widehat{B}(q)$. To derive this, we define $\tilde{\xi}(q) = \{\mathcal{G}[B\psi]_\alpha(q+K)\}_{K\alpha\in\Omega^*}$. We then utilize (10) to find

$$\mathcal{G}[AB\psi](q) = \widehat{A}(q)\tilde{\xi}(q) = \widehat{A}(q)\widehat{B}(q)\xi(q) \tag{13}$$

where $[\xi(q)]_{K\alpha} = \mathcal{G}\psi_\alpha(q+K)$. We showed in [11] that

$$\begin{aligned}\lim_{r\to\infty}\frac{1}{\#\Omega_r}\mathrm{Tr}_{\Omega_r}[\phi(H)] &= \lim_{r\to\infty}\frac{1}{\#\Omega_r^*}\mathrm{Tr}_{\Omega_r^*}[\phi(\widehat{H}(q^*))]\\ &= \nu^*\sum_{k=1}^{2}\sum_{\alpha\in\mathcal{A}_k}\int_{\Gamma_k^*}[\phi(\widehat{H}(q))]_{0\alpha,0\alpha}dq\end{aligned} \tag{14}$$

for all polynomials $\phi(E)$ and $q^* \in \mathbb{R}^2$, and where

$$\nu^* = \frac{1}{\sum_{k=1}^{2}|\Gamma_k^*|\cdot(\#\mathcal{A}_k)}$$

and Ω_r^* is the finite domain in momentum space

$$\Omega_r^* = \Omega_{1r}^* \cup \Omega_{2r}^* := ((\mathcal{R}_2^* \cap B_r)\times\mathcal{A}_1) \cup ((\mathcal{R}_1^* \cap B_r)\times\mathcal{A}_2).$$

We can now apply (14) and then subsequently (13) to obtain that

$$\begin{aligned}&\int\phi(E)\psi(E')d\mu_{ij}(E,E')\\ &= \lim_{r\to\infty}\frac{1}{\#\Omega_r}\mathrm{Tr}_{\Omega_r}[\phi(H)[X_i,H]\psi(H)[X_j,H]]\\ &= \nu^*\sum_{k=1}^{2}\sum_{\alpha\in\mathcal{A}_k}\int_{\Gamma_k^*}\left[\left(\phi(H)[X_i,H]\psi(H)[X_j,H]\right)^\wedge(q)\right]_{0\alpha,0\alpha}dq\\ &= \nu^*\sum_{k=1}^{2}\sum_{\alpha\in\mathcal{A}_k}\int_{\Gamma_k^*}[\phi(\widehat{H}(q))\partial_i\widehat{H}(q)\psi(\widehat{H}(q))\partial_j\widehat{H}(q)]_{0\alpha,0\alpha}\,dq\end{aligned} \tag{15}$$

for all polynomials $\phi(E)$, $\psi(E)$. We are now in a position to define the momentum space current-current correlation measure, $\mu_{ij}^*(E,E')$ by

$$\begin{aligned}&\int\phi(E)\psi(E')d\mu_{ij}^*(E,E')\\ &= \nu^*\sum_{k=1}^{2}\sum_{\alpha\in\mathcal{A}_k}\int_{\Gamma_k^*}[\phi(\widehat{H}(q))\partial_i\widehat{H}(q)\psi(\widehat{H}(q))\partial_j\widehat{H}(q)]_{0\alpha,0\alpha}dq\end{aligned} \tag{16}$$

for all polynomials $\phi(E)$ and $\psi(E')$. Then by (15) we obtain that the real space and momentum space current-current correlation meaures are identical,

$$\mu_{ij} = \mu^*_{ij}. \tag{17}$$

We can thus immediately transform the Kubo formula (5) into our momentum space formulation using (15) to obtain

$$\sigma_{ij} = \int F(E,E')d\mu^*_{ij}(E,E'). \tag{18}$$

4 Algorithm

In this section, we will assume the two materials have similar lattice sizes, i.e., $A_1 \approx A_2$, and we'll be interested in low temperature and large relaxation times. In this regime, real space and supercell approximations become expensive [8,15,16]. In contrast, in momentum space we will show that only small matrix calculations are required, which allows a rapid full diagonalization. We also will assume frequency is low so that higher energy modes are negligible. As defined above, σ_{ij} still requires the computation of a diagonal entry for an operator on an infinite-dimensional Hilbert space. To develop a computational method, we define the injection operator by

$$[P_r\xi]_{K\alpha} = \xi_{K\alpha}\delta_{K\alpha\in\Omega^*_r}.$$

For an operator A defined over the Hilbert space $\ell^2(\Omega^*)$, we can compute the matrix $A_r = P^*_r A P_r$.

This will be used to restrict an infinite-dimensional operator A to a finite-dimensional matrix. Indeed, we can approximate the current-current correlation measure, $\mu^r_{ij}(E,E')$, by

$$\begin{aligned}\int \phi(E)\psi(E')d\mu^r_{ij}(E,E') \\ = \nu^* \sum_{k=1}^{2}\sum_{\alpha\in\mathcal{A}_k}\int_{\Gamma^*_k}[\phi(\widehat{H}_r(q))\partial_i\widehat{H}_r(q)\psi(\widehat{H}_r(q)) \\ \times \partial_j\widehat{H}_r(q)]_{0\alpha,0\alpha}dq\end{aligned} \tag{19}$$

and the approximate conductivity by

$$\sigma^r_{ij} = \int F(E,E')d\mu^r_{ij}(E,E'). \tag{20}$$

When we are interested in long relaxation times and low temperatures, the momentum space approach converges very quickly for many materials of interest such as twisted bilayer graphene as discussed at the end of the section. Indeed, it converges so quickly that accurate results may be obtained for r significantly less than the moiré length scale $\|A_1^{-T} - A_2^{-T}\|^{-1}$. For example, in tBLG only wavenumbers q near the Dirac points will contribute strongly to conductivity. As a consequence of this convergence, we can reduce the domain of integration Γ^*_k in (19) to write a more efficient algorithm related to that used in [9]. In particular, our Hamiltonian can be defined over a grid of q-points based off the *incommensurate supercell* reciprocal lattice

$$\mathcal{R}^*_{12} = 2\pi(A_1^{-T} - A_2^{-T})\mathbb{Z}^2. \tag{21}$$

This motivates us to define its unit cell of the *incommensurate* reciprocal moiré superlattice centered at $\tilde{q}$ to be

$$\Gamma^*_{12}(\tilde{q}) = \{\tilde{q} + 2\pi(A_1^{-T} - A_2^{-T})\zeta : \zeta \in [0,1)^2\}, \tag{22}$$

where $\tilde{q}$'s will be chosen to center our regions where the integrand in (19) is significant. In the case of tBLG, we would consider two $\tilde{q}$'s near the Dirac points. One point would be chosen near the K points for the two sheets and the other near the K' points for the two sheets.

We denote (v_m, E_m) as the eigenpairs of $\widehat{H}_r(q)$ where q is suppressed from the notation for brevity's sake. Then $\widehat{H}_r(q) = \sum_m E_m v_m v^*_m$. Then we can derive

$$\begin{aligned}\tilde{\sigma}^r_{ij} = \nu^* \sum_{\tilde{q}}\int_{\Gamma^*_{12}(\tilde{q})}\sum_{m,m'} F(E_m,E_{m'}) \\ \times \mathrm{Tr}[v_m v^*_m \partial_i\widehat{H}_r(q) v_{m'} v^*_{m'}\partial_j\widehat{H}_r(q)]dq.\end{aligned} \tag{23}$$

See Section A.3 for the derivation. To numerically approximate $\partial_i\widehat{H}_r(q)$, we can use any standard single variable differentiation scheme such as the centered midpoint formula to compute the derivative matrix. Note that we simply store the matrix directly, and no eigen-decomposition is used. Finally, the integral is evaluated by discretization using a uniform mesh over the entire incommensurate supercell Brillouin zone.

Our algorithm can achieve an exponential rate of convergence when applied to many 2D heterostructures. First we need $\|A_1^{-T} - A_2^{-T}\|$ to be small, which is an assumption we have used throughout this section, and applies to the small twist regimes in bilayers of the same material. We further require that the Fermi energy roughly corresponds to a non-flat band regime for the monolayers. It applies well to regions with parabolic bands or Dirac points. From a technical perspective, one must look at the collection of level sets of the monolayer band structures in terms of energy (See [11] for details).

We next consider the rate of convergence for our algorithm to compute the conductivity for such 2D heterostructures. It has been shown [7] that the Green's functions of these Hamiltonians decay exponentially fast in this energy window. As a consequence, we expect that if the 2D materials and the Fermi level are as described above, we have the following rate of convergence for the our approximate conductivity to the exact Kubo conductivity:

$$|\tilde{\sigma}^r_{ij} - \sigma_{ij}| \le p(\zeta)e^{-\gamma r} \tag{24}$$

where $\zeta = \max\{\beta, \eta^{-1}\}$, the decay rate $\gamma > 0$ is independent of ε, and p is a polynomial derived from the error analysis. The proof of this estimate follows from the same

Green's function decay estimates found in Theorem 3.1 of [11]. We do not address the proof here, but we do provide numerical evidence for this decay rate in Figure 2 for the tBLG case (see Sect. 5). Note that in this numerical example the true solution is computed by a momentum space calculation, not a real space calculation. We justify this choice by using our derived formula (18), which implies equivalence of the thermodynamic limit of momentum space and real space conductivity formulations.

The outline of the algorithm is then the following:

- Find the required $\tilde{q}$'s corresponding to points near parabolic band centers or Dirac points.
- Build $\widehat{H}_r(Q_N)$ and $\partial_i \widehat{H}_r(Q_N)$ using (8) and (9) for $\{Q_N\}$ a uniform discretization of $\Gamma^*_{12}(\tilde{q})$.
- Compute eigenvectors and eigenvalues of $\widehat{H}_r(Q_N)$.
- Compute the conductivity $\tilde{\sigma}^r_{ij}$ from (23).

We observe that this algorithm is highly parallel in the Q_N discretization and critical points $\tilde{q}$.

5 Numeric example: tBLG

Applying this method to tBLG provides validation of the scheme numerically and physically interpretable results. For construction of the momentum Hamiltonian of tBLG, the only challenging ingredient is the Fourier transform of the interlayer coupling, $\hat{h}$. A square-grid FFT is not ideal as it may violate the three-fold rotational or sublattice exchange symmetries still present in the twisted geometry. We therefore directly compute components of $\hat{h}$ on a triangular grid and ensure our interpolation respects the appropriate crystal symmetry. As we are performing a discretization of momenta, Q_N, the singular nature of $F(E, E')$ even at finite ω is regularized by the size of η. We use a 60×60 mesh sampling of Q_N around each copy of the moiré Brillouin zone, finding this sufficient to obtain the key physical results for tBLG with twist angle larger than 1°. A value of η corresponding to the relaxation time of graphene ($\eta \approx 10^{-6}$ eV) is too small to give smooth results in this case. Instead, η is taken on the order of 10^{-2} eV, and is a tunable parameter to ensure sufficient smoothness in the resulting $\sigma(\omega)$ curve. For a finer mesh of Q_N, or if a finite element approach for interpolating between q points is used, η can be made smaller.

All results are normalized in units of the conductance of monolayer graphene, which is nearly frequency-independent for $E_F < \hbar\omega \ll 3$ eV with a value of $\sigma_0 = \frac{1}{4}\frac{e^2}{\hbar}$ (it is exactly frequency-independent in the Dirac cone approximation) [14]. As tBLG has time-reversal symmetry, only σ_{xx} and σ_{yy} can be non-zero, and taking into account the three-fold rotational symmetry one must have $\sigma_{xx} = \sigma_{yy}$. As a consequence, the current–current correlation measure $d\mu$ is purely real, and σ can be decomposed into its real and imaginary part by manipulating $F(E, E')$. This leads to $\mathrm{Im}(\sigma)$ not having any dependence on $f_\beta(E)$, and thus necessitating a sum over all states of the tBLG system, which removes the advantage of the momentum space method. Such a divergence can be partly corrected with a "cancellation of infinities" [12], but here we focus instead on the real part. Thus, all results are given in normalized units of $\mathrm{Re}(\sigma)/\sigma_0$.

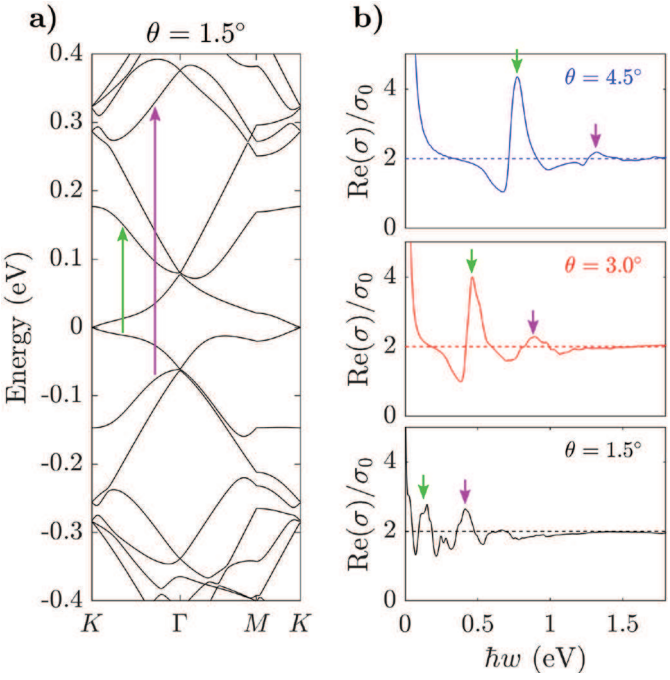

Fig. 1. (a) Band structure of tBLG for $\theta = 1.5°$. The green and purple arrows highlight the interband transitions important in the conductivity calculation. (b) Real part of the conductivity, $Re(\sigma(0,\omega))$, normalized by $\sigma_0 = \frac{1}{4}\frac{e^2}{\hbar}$, for three different twist angles and $T = 0.3$ K. The two inter band transitions are marked with small arrows, matching the band structure arrows. The background value for a decoupled bilayer, $2\sigma_0$, is shown with a dashed line.

In Figure 1b, we calculate $\sigma(E_F, \omega)$ for various ω and with E_F fixed at the charge neutrality point, which is set to 0 eV. Evaluating $\sigma(0, \omega)$ returns reasonable results for three choices of θ, with two clear peaks in the conductivity in each case. These two peaks are associated with the interband transitions highlighted with the arrows in the band structure of Figure 1a. There is also a large divergence in $\mathrm{Re}(\sigma)$ as $\omega \to 0$, which is a result of the singularity inherent in the definition of $F(E, E')$.

We next study the convergence of the conductivity as the momentum truncation radius is increased in Figure 2. Excellent agreement to (24) is observed, with an exponential decay with factor $\gamma = 1.25$ Å at all relevant energy values. Such convergence ensures accuracy of the conductivity even for highly truncated momentum Hamiltonians, and allows the algorithm to produce quality results even on a laptop. Compared to real space approaches, which require large amounts of memory and processing power due to the weak convergence in their truncation radius [8], this is a significant improvement.

Turning now to the dependence of σ on E_F, we fix ω to the value of the first interband transition of $\theta = 3.0°$ and sweep E_F in Figure 3b. Comparing the result to the band structure at the same twist angle, it is clear that the interband tranistion is strongest at the charge neutrality point, and quickly falls off as one approaches the edges of any

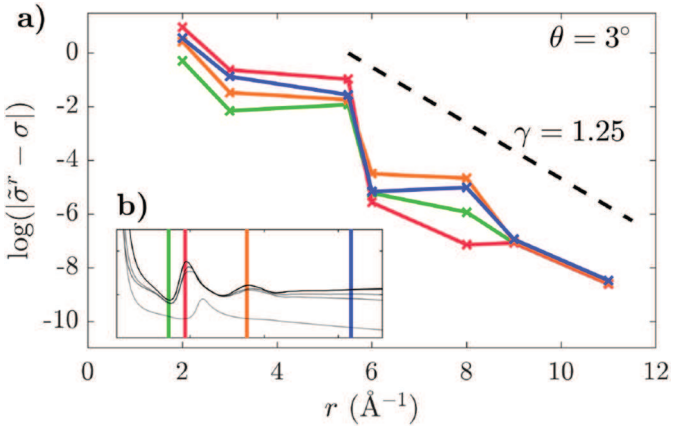

Fig. 2. (a) Error in the conductivity of the approximate model, $\tilde{\sigma}^r$, as a function of truncation radius in momentum space, r, for four different choices of ω for a twist angle of $\theta = 3°$. The conductivity obtained with a truncation radius of $r = 13$ Å^{-1} is taken as the true value, σ. Only the real part of the conductivity is considered, in units of σ_0, and with the same settings as in Figure 1b. Each colored curve corresponds to a specific ω given in the inset, and an error dependence of $e^{-\gamma r}$ with $\gamma = 1.25$ Å plotted as a dashed black line. (b) Real part of the conductivity, $Re(\sigma(0,\omega))$, for 3° twist angle. For axis units, see Figure 1b. The opacity of the curves indicate their truncation radius, with the darkest (lightest) line corresponding to 13 Å^{-1} (2 Å^{-1}). The colored vertical lines give the ω values for the four colored error curves in panel (a).

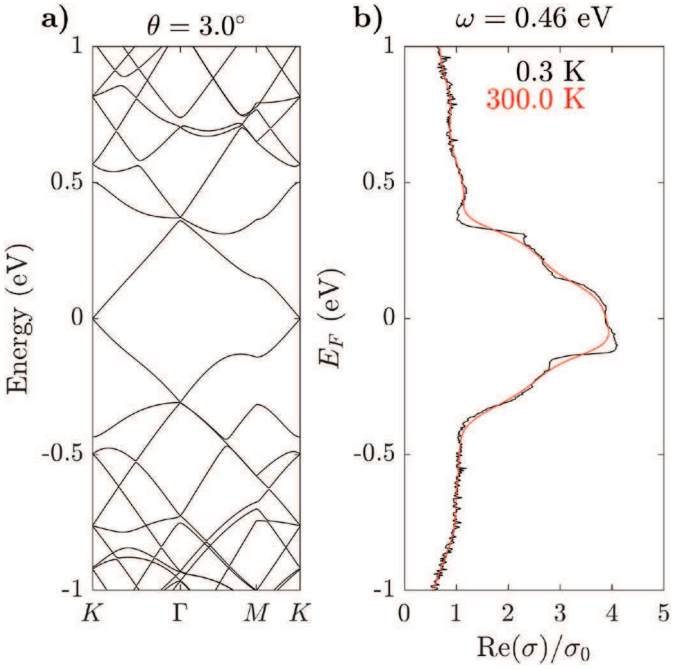

Fig. 3. (a) Band structure of tBLG for $\theta = 3.0°$. **b)** Real part of the conductivity, $Re(\sigma(E_F,\omega))$, normalized by $\sigma_0 = \frac{1}{4}\frac{e^2}{\hbar}$ as a function of the Fermi energy. The black (red) line corresponds to $T = 0.3$ K (300 K).

bands associated with that specific interband transition. Changing the temperature from 0.3 K to 300 K smooths the features of Re(σ), but otherwise has no effect.

The twist-dependent interband transitions and saturation of the conductivity to a nearly constant value at large frequency are well understood linear-response phenomena in TBLG [12,13]. Their recovery in our formulation is proof that not only the method converges, but that it converges to a correct result. This physical demonstration complements our numeric convergence to demonstrate our algorithm's accuracy.

6 Conclusion

In this paper, we introduced an efficient algorithm for computing conductivity in a momentum space framework and demonstrate its effectiveness for tBLG. For applicable 2D heterostructures, the algorithm's computationally complexity will be far less than that of real space approaches, and bypasses the need for commensurate supercells. We derived the momentum space model and Kubo formula directly from the real space formulation.

The momentum space framework is very generalizable and versatile in applicability, generalizing to many incommensurate 2D systems including twisted bilayer with mechanical relaxation [17], and even trilayers, and providing a foundation for the development of efficient and accurate methods to compute the Kubo conductivity in 2D heterostructures.

DM, SC, and ML were supported in part by ARO MURI Award W911NF-14-1-0247. ML was also supported in part by NSF grants DMS-1906129 and DMR-1922165, and SC was supported in part by NSF grant DMR-1231319.

Author contribution statement

All authors contributed equally to the development of the model. D.M. led the writing and analysis and S.C. led the application of the algorithm.

Appendix A

A.1 Derivation of (10)

We can verify (10) for intralayer coupling by setting $\alpha \in \mathcal{A}_1$ and observing that

$$
\begin{aligned}
&[\mathcal{G}_1 H(\psi_1, 0)^T]_\alpha(q) \\
&= |\Gamma_1^*|^{-1/2} \sum_{R\in\mathcal{R}_1} e^{-iq\cdot R} \sum_{R'\alpha'\in\Omega_1} H_{R\alpha,R'\alpha'}\psi_{R'\alpha'} \\
&= |\Gamma_1^*|^{-1/2} \sum_{R\in\mathcal{R}_1} e^{-iq\cdot R} \sum_{R'\alpha'\in\Omega_1} h_{\alpha\alpha'}(R-R')\psi_{R'\alpha'} \\
&= |\Gamma_1^*|^{-1/2} \left(\sum_{R\in\mathcal{R}_1} e^{-iq\cdot R} h_{\alpha\alpha'}(R)\right)\left(\sum_{R'\in\mathcal{R}_1} e^{-iq\cdot R'}\psi_{R'\alpha'}\right) \\
&= |\Gamma_1^*|^{1/2} \mathcal{G}_1 h_{\alpha\alpha'}(q)\mathcal{G}_1\psi_{\alpha'}(q),
\end{aligned}
$$

which gives (10) for the intralayer coupling in momentum space (8).

Next we consider interlayer coupling. Letting $\alpha \in \mathcal{A}_1$ again, we have that

$$\begin{aligned}
&[\mathcal{G}_1 H(0,\psi_2)^T]_\alpha(q)\\
&= |\Gamma_1^*|^{-1/2} \sum_{R\in\mathcal{R}_1} e^{-iq\cdot R} \sum_{R'\alpha'\in\Omega_2} H_{R\alpha,R'\alpha'}\psi_{R'\alpha'}\\
&= |\Gamma_1^*|^{-1/2} \sum_{R\in\mathcal{R}_1} e^{-iq\cdot R} \sum_{R'\alpha'\in\Omega_2} h_{\alpha\alpha'}(R-R')\psi_{R'\alpha'}\\
&= |\Gamma_1^*|^{-1/2} \sum_{R\in\mathcal{R}_1} e^{-iq\cdot R} \sum_{R'\alpha'\in\Omega_2} \int \hat{h}_{\alpha\alpha'}(\zeta) e^{i\zeta\cdot(R-R')}\, d\zeta\, \psi_{R'\alpha'}\\
&= |\Gamma_1^*|^{1/2}|\Gamma_2^*|^{1/2} \sum_{K\in\mathcal{R}_1^*}\sum_{\alpha'\in\mathcal{A}_2} \int \hat{h}_{\alpha\alpha'}(\zeta)\delta(\zeta-q-K)\mathcal{G}\psi_{\alpha'}(\zeta)\, d\zeta\\
&= |\Gamma_1^*|^{1/2}|\Gamma_2^*|^{1/2} \sum_{K\in\mathcal{R}_1^*} \hat{h}_{\alpha\alpha'}(q+K)\mathcal{G}_2\psi_{\alpha'}(q+K)
\end{aligned}$$

by the Poisson summation formula $\sum_{R\in\mathcal{R}_1} e^{i(\zeta-q)\cdot R} = |\Gamma_1^*| \sum_{K\in\mathcal{R}_1^*} \delta(\zeta-q-K)$ which gives (10) for the interlayer coupling in momentum space (9).

A.2 Derivation of (11).

To derive the Bloch transform of the current operator (11), we first let $\alpha \in \mathcal{A}_1$ and consider the intralayer interaction. We have

$$\begin{aligned}
&[\mathcal{G}_1[X_j, H](\psi_1,0)^T]_\alpha(q)\\
&= |\Gamma_1^*|^{-1/2} \sum_{R\in\mathcal{R}_1} e^{-iq\cdot R} \sum_{R'\alpha'\in\Omega_1} [R_j - R'_j] H_{R\alpha,R'\alpha'}\psi_{R'\alpha'}\\
&= |\Gamma_1^*|^{-1/2} \sum_{R\in\mathcal{R}_1} e^{-iq\cdot R} \sum_{R'\alpha'\in\Omega_1} [R_j - R'_j] h_{\alpha\alpha'}(R-R')\psi_{R'\alpha'}\\
&= |\Gamma_1^*|^{-1/2} \left(\sum_{R\in\mathcal{R}_1} e^{-iq\cdot R} R_j h_{\alpha\alpha'}(R)\right)\left(\sum_{R'\in\mathcal{R}_1} e^{-iq\cdot R'}\psi_{R'\alpha'}\right)\\
&= i|\Gamma_1^*|^{-1/2} \left(\sum_{R\in\mathcal{R}_1} \partial_j e^{-iq\cdot R} h_{\alpha\alpha'}(R)\right)\left(\sum_{R'\in\mathcal{R}_1} e^{-iq\cdot R'}\psi_{R'\alpha'}\right)\\
&= i|\Gamma_1^*|^{1/2}\partial_j \mathcal{G}_1 h_{\alpha\alpha'}(q)\mathcal{G}_1\psi_{\alpha'}(q).
\end{aligned} \tag{A.1}$$

Next, we consider interlayer coupling and let $\alpha \in \mathcal{A}_1$ again to derive

see equation (A.2) next page.

Putting these derivations for intralayer and interlayer coupling together gives the final result (11).

A.3 Derivation of (23)

It is useful at this point to define in parallel to (19) approximate and exact *local conductivities* in momentum space given by the local correlation measure defined by

$$\begin{aligned}
&\int \phi(E)\psi(E')d\mu^r_{ij,K\alpha}[q](E,E')\\
&\qquad = [\phi(\widehat{H}_r(q))\partial_i\widehat{H}_r(q)\psi(\widehat{H}_r(q))\partial_j\widehat{H}_r(q)]_{K\alpha,K\alpha},
\end{aligned} \tag{A.3}$$

$$\begin{aligned}
&\int \phi(E)\psi(E')d\mu_{ij,K\alpha}[q](E,E')\\
&\qquad = [\phi(\widehat{H}(q))\partial_i\widehat{H}(q)\psi(\widehat{H}(q))\partial_j\widehat{H}(q)]_{K\alpha,K\alpha}.
\end{aligned} \tag{A.4}$$

The local conductivity and its approximation are then defined by

$$\sigma^r_{ij,K\alpha}[q] = \int F(E,E')d\mu^r_{ij,K\alpha}[q](E,E'), \tag{A.5}$$

$$\sigma_{ij,K\alpha}[q] = \int F(E,E')d\mu_{ij,K\alpha}[q](E,E'), \tag{A.6}$$

and the global conductivity and its approximation are given by

$$\sigma^r_{ij} = \nu^* \sum_{k=1}^{2}\sum_{\alpha\in\mathcal{A}_k} \int_{\Gamma_k^*} \sigma^r_{ij,0\alpha}[q]dq, \tag{A.7}$$

$$\sigma_{ij} = \nu^* \sum_{k=1}^{2}\sum_{\alpha\in\mathcal{A}_k} \int_{\Gamma_k^*} \sigma_{ij,0\alpha}[q]dq. \tag{A.8}$$

We denote $P_1 = 2$ and $P_2 = 1$. For $K\alpha \in \Omega_k^*$ such that $K = 2\pi A_{P_k}^{-T} n$ where $n = (n_1, n_2)^T$ is a pair of integers, we define

$$q_n = 2\pi(A_{P_k}^{-T} - A_k^{-T})n. \tag{A.9}$$

We have the identity

$$\sigma_{ij,K\alpha}[q] = \sigma_{ij,0\alpha}[q+q_n]. \tag{A.10}$$

See Section A.4 for the derivation of this result. We additionally have the approximation

$$\sigma^r_{ij,K\alpha}[q] \approx \sigma^r_{ij,0\alpha}[q+q_n]. \tag{A.11}$$

An important factor in the validation of this approximation is that only energies near the Fermi energy contribute to conductivity, at least to leading order. This is because $F(E,E')$ to leading order is dominated by $E \approx E' \approx E_F$. Consider sheet j as a monolayer for a moment. Suppose $\varepsilon_n^j(q)$ is the n^{th} eigenvalue corresponding to wavenumber q. Then it turns out only wavenumbers q with corresponding eigenvalues $\varepsilon_n^j(q)$ near the Fermi energy contribute strongly to conductivity *in the bilayer case*. In other words, monolayer band structure informs what wavenumbers are relevant for the bilayer system. In the case of tBLG, only wavenumbers near the Dirac cones contribute strongly when the Fermi energy is near the Dirac point. For local conductivity, this means $\sigma_{ij,0\alpha}[q]$ becomes small if $\varepsilon_n^j(q)$ is sufficiently far from the Fermi energy for all n. This gives us a reduced space of wavenumbers we need to consider.

$$
\begin{aligned}
[\mathcal{G}_1[X_j,H](0,\psi_2)^T]_\alpha(q) &= |\Gamma_1^*|^{-1/2}\sum_{R\in\mathcal{R}_1} e^{-iq\cdot R}\sum_{R'\alpha'\in\Omega_2}(R_j-R'_j)H_{R\alpha,R'\alpha'}\psi_{R'\alpha'}\\
&= |\Gamma_1^*|^{-1/2}\sum_{R\in\mathcal{R}_1} e^{-iq\cdot R}\sum_{R'\alpha'\in\Omega_2}(R_j-R'_j)h_{\alpha\alpha'}(R-R')\psi_{R'\alpha'}\\
&= |\Gamma_1^*|^{-1/2}\sum_{R\in\mathcal{R}_1} e^{-iq\cdot R}\sum_{R'\alpha'\in\Omega_2}(R_j-R'_j)\int \hat{h}_{\alpha\alpha'}(\zeta)e^{i\zeta\cdot(R-R')}d\zeta\psi_{R'\alpha'}\\
&= i|\Gamma_1^*|^{-1/2}\sum_{R\in\mathcal{R}_1} e^{-iq\cdot R}\sum_{R'\alpha'\in\Omega_2}\int \partial_j\hat{h}_{\alpha\alpha'}(\zeta)e^{i\zeta\cdot(R-R')}d\zeta\psi_{R'\alpha'}\\
&= i|\Gamma_1^*|^{1/2}|\Gamma_2^*|^{1/2}\sum_{K\in\mathcal{R}_1^*}\sum_{\alpha'\in\mathcal{A}_2}\int \partial_j\hat{h}_{\alpha\alpha'}(\zeta)\delta(\zeta-q-K)\mathcal{G}\psi_{\alpha'}(\zeta)d\zeta\\
&= i|\Gamma_1^*|^{1/2}|\Gamma_2^*|^{1/2}\sum_{K\in\mathcal{R}_1^*}\partial_j\hat{h}_{\alpha\alpha'}(q+K)\mathcal{G}_2\psi_{\alpha'}(q+K)
\end{aligned}
\tag{A.2}
$$

As described above, the local conductivity $\sigma^r_{ij,0\alpha}[q]$ is small for q far from the $\tilde{q}$ points. As such, we can approximate integrals of $\sigma^r_{ij,0\alpha}[q]$ over the Brillouin zones Γ_k^* by integrals over the much smaller isolated regions defined by the sets

$$
\Gamma^*(\tilde{q},k) = \bigcup_{\{n:|2\pi A_{P_k}^{-T}n|<r\}}\left(\Gamma_{12}^*(\tilde{q})+2\pi(A_{P_k}^{-T}-A_k^{-T})n\right). \tag{A.12}
$$

See Figure A.1.

Using these approximations, we have

$$
\sigma^r_{ij}\approx\nu^*\sum_{\tilde{q}}\int_{\Gamma_{12}^*(\tilde{q})}\sum_{K\alpha\in\Omega_r^*}\sigma^r_{ij,K\alpha}[q]dq. \tag{A.13}
$$

See Section A.5 for the derivation. The sum in the integrand is simply a trace, which motivates us to define an approximate measure $\tilde{\mu}^r_{ij}$ by

$$
\begin{aligned}
&\int\phi(E)\psi(E')d\tilde{\mu}^r_{ij}(E,E')\\
&=\nu^*\sum_{\tilde{q}}\int_{\Gamma_{12}^*(\tilde{q})}\mathrm{Tr}[\phi(\widehat{H}_r(q))\partial_i\widehat{H}_r(q)\psi(\widehat{H}_r(q))\partial_j\widehat{H}_r(q)]dq.
\end{aligned}
\tag{A.14}
$$

Here we sum over the relevant regions via $\tilde{q}$. For simplicity, we are assuming that the approximating integration domains are centered around points as in $\Gamma_{12}^*(\tilde{q})$, though this framework can be generalized beyond such restrictions [11]. We now have the corresponding approximate Kubo formula:

$$
\tilde{\sigma}^r_{ij}=\int F(E,E')d\tilde{\mu}^r_{ij}(E,E'). \tag{A.15}
$$

Recall (v_m,E_m) are the eigenpairs of $\widehat{H}_r(q)$ where q is suppressed from the notation for brevity's sake. Then

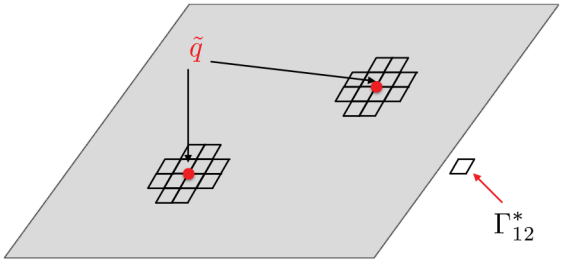

Fig. A.1. The grey large cell is Γ_1^*. Here $\Gamma_{12}^*=2\pi(A_1^{-T}-A_2^{-T})[0,1)^2$, a sample of the supercell reciprocal lattice unit cell. Each bottom-left vertex of the parallelograms around the $\tilde{q}$ points represent $\tilde{q}+q_n$ positions. Hence the decomposition given by (A.12) breaks the regions around the $\tilde{q}$ points into a union of small parallelograms.

$\widehat{H}_r(q)=\sum_m E_m v_m v_m^*$. As a consequence, we have

$$
\begin{aligned}
\tilde{\sigma}^r_{ij} = \nu^*\sum_{\tilde{q}}\int_{\Gamma_{12}^*(\tilde{q})}\sum_{m,m'}F(E_m,E_{m'})\\
\times\mathrm{Tr}[v_m v_m^*\partial_i\widehat{H}_r(q)v_{m'}v_{m'}^*\partial_j\widehat{H}_r(q)]dq.
\end{aligned}
\tag{A.16}
$$

A.4 Derivation of (A.10)

To show this, suppose $\alpha\in\mathcal{A}_1$. Then let T_K ($K=2\pi A_2^{-T}n$) be the translation of sheet 1 operator defined by

$$
[T_K\xi]_{K'\alpha'}=\xi_{(K'-K)\alpha'}\text{ if }\alpha'\in\mathcal{A}_1, \tag{A.17}
$$

$$
[T_K\xi]_{K'\alpha'}=\xi_{(K'+2\pi A_1^{-T}n)\alpha'}\text{ if }\alpha'\in\mathcal{A}_2. \tag{A.18}
$$

Now we observe

$$
T_K^*\widehat{H}(q)T_K=\widehat{H}(q+q_n). \tag{A.19}
$$

Note we defined the translation T_K in such a way that as $n \in \mathbb{Z}^2$ varies, $\widehat{H}(q+q_n)$ varies slowly. We next observe

$$\begin{aligned}
&[\phi(\widehat{H}(q))\partial_i\widehat{H}(q)\psi(\widehat{H}(q))\partial_j\widehat{H}(q)]_{K\alpha,K\alpha}\\
&= [T_K^*\phi(\widehat{H}(q))\partial_i\widehat{H}(q)\psi(\widehat{H}(q))\partial_j\widehat{H}(q)T_K]_{0\alpha,0\alpha}\\
&= [\phi(T_K^*\widehat{H}(q)T_K)T_K^*\partial_i\widehat{H}(q)T_K\psi(T_K^*\widehat{H}(q)T_K)T_K^*\partial_j\widehat{H}(q)T_K]_{0\alpha,0\alpha}\\
&= [\phi(\widehat{H}(q+q_n))\partial_i\widehat{H}(q+q_n)\psi(\widehat{H}(q+q_n))\partial_j\widehat{H}(q+q_n)]_{0\alpha,0\alpha}.
\end{aligned}$$

Since this holds for the local current-current correlation, it extends to local conductivity.

A.5 Derivation of (A.13)

We have

$$\begin{aligned}
\sigma_{ij}^r &= \nu^* \sum_{k=1}^{2} \sum_{\alpha\in\mathcal{A}_k} \int_{\Gamma_k^*} \sigma_{ij,0\alpha}^r[q]dq\\
&\approx \nu^* \sum_{k=1}^{2} \sum_{\alpha\in\mathcal{A}_k} \sum_{\tilde{q}} \int_{\Gamma_k^*(\tilde{q},k)} \sigma_{ij,0\alpha}^r[q]dq\\
&= \nu^* \sum_{k=1}^{2} \sum_{\alpha\in\mathcal{A}_k} \sum_{K\in\mathcal{R}_{P_k}^*\cap B_r} \sum_{\tilde{q}} \int_{\Gamma_{12}^*(\tilde{q})} \sigma_{ij,0\alpha}^r[q+q_n]dq\\
&\approx \nu^* \sum_{k=1}^{2} \sum_{\alpha\in\mathcal{A}_k} \sum_{K\in\mathcal{R}_{P_k}^*\cap B_r} \sum_{\tilde{q}} \int_{\Gamma_{12}^*(\tilde{q})} \sigma_{ij,K\alpha}^r[q]dq\\
&= \nu^* \sum_{\tilde{q}} \int_{\Gamma_{12}^*(\tilde{q})} \sum_{K\alpha\in\Omega_r^*} \sigma_{ij,K\alpha}^r[q]dq.
\end{aligned}$$

References

1. Y. Cao, V. Fatemi, S. Fang, K. Watanabe, T. Taniguchi, E. Kaxiras, P. Jarillo-Herrero, Nature **556**, 43 (2018)
2. S. Carr, D. Massatt, S. Fang, P. Cazeaux, M. Luskin, E. Kaxiras, Phys. Rev. B **95**, 075420 (2017)
3. A.K. Geim, I.V. Grigorieva, Nature **499**, 419 (2013)
4. A.H. Castro Neto, F. Guinea, N.M.R. Peres, K.S. Novoselov, A.K. Geim, Rev. Mod. Phys. **81**, 109 (2009)
5. S. Das, J.A. Robinson, M. Dubey, H. Terrones, M. Terrones, Ann. Rev. Mater. Res. **45**, 1 (2015)
6. E. Cancès, P. Cazeaux, M. Luskin, J. Math. Phys. **58**, 063502 (2017)
7. D. Massatt, M. Luskin, C. Ortner, Multiscale Model. Simul. **15**, 476 (2017)
8. S. Etter, D. Massatt, M. Luskin, C. Ortner, arXiv:1907.01314 (2019)
9. R. Bistritzer, A.H. MacDonald, Proc. Natl. Acad. Sci. **108**, 12233 (2011)
10. G. Catarina, B. Amorim, E.V. Castro, J.M.V.P. Lopes, N. Peres, Twisted Bilayer Graphene: Low?Energy Physics, Electronic and Optical Properties, in *Handbook of Graphene Set*, edited by E. Celasco, A.N. Chaika, T. Stauber, M. Zhang, C. Ozkan, C. Ozkan, U. Ozkan, B. Palys, S.W. Harun (2019), doi:10.1002/9781119468455.ch44
11. D. Massatt, S. Carr, M. Luskin, C. Ortner, SIAM J. Multiscale Model. Simul. **16**, 429 (2018)
12. T. Stauber, P. San-Jose, L. Brey, New J. Phys. **15**, 113050 (2013)
13. P. Moon, Y.W. Son, M. Koshino, Phys. Rev. B **90**, 155427 (2014)
14. T. Stauber, N.M.R. Peres, A.K. Geim, Phys. Rev. B **78**, 085432 (2008)
15. H.A. Le, V.N. Do, Phys. Rev. B **97**, 125136 (2018)
16. A. Vela, M.V.O. Moutinho, F.J. Culchac, P. Venezuela, R.B. Capaz, Phys. Rev. B **98**, 155135 (2018)
17. S. Carr, D. Massatt, S.B. Torrisi, P. Cazeaux, M. Luskin, E. Kaxiras, Phys. Rev. B, **98**, 224102 (2018)
18. H. Yoo, R. Engelke, S. Carr, S. Fang, K. Zhang, P. Cazeaux, S.H. Sung, R. Hovden, A.W. Tsen, T. Taniguchi et al., Nat. Mater. **18**, 448 (2019)
19. P. Cazeauz, M. Luskin, D. Massatt, Arch. Rat. Mech. Anal. **235**, 1289 (2019)
20. C. Mora, N. Regnault, B.A. Bernevig, Phys. Rev. Lett. **123**, 026402 (2019)